HHS Public Access

Author manuscript

Oncogene. Author manuscript; available in PMC 2019 January 01.

Published in final edited form as:

Oncogene. 2018 July ; 37(28): 3763–3777. doi:10.1038/s41388-018-0194-3.

BRD4 facilitates replication stress-induced DNA damage response

Jingwen Zhang[#1], **Austin M. Dulak**[#1], **Maureen M. Hattersley**[1], **Brandon S. Willis**[1], **Jenni Nikkilä**[2], **Anderson Wang**[2], **Alan Lau**[2], **Corinne Reimer**[1], **Michael Zinda**[1], **Stephen E. Fawell**[1], **Gordon B. Mills**[3], and **Huawei Chen**[1]

[1]Oncology, IMED Biotech Unit, AstraZeneca, Boston, , USA

[2]Oncology, IMED Biotech Unit, AstraZeneca, Cambridge, United Kingdom

[3]Department of Systems Biology, The University of Texas MD Anderson Cancer Center, Houston, TX 77030, USA

[#] These authors contributed equally to this work.

Abstract

Previous reports have demonstrated that select cancers depend on BRD4 to regulate oncogenic gene transcriptional programs. Here, we describe a novel role for BRD4 in DNA damage response (DDR). BRD4 associates with and regulates the function of pre-replication factor CDC6 and plays an indispensable part in DNA replication checkpoint signaling. Inhibition of BRD4 by JQ1 or AZD5153 resulted in a rapid, time-dependent reduction in CHK1 phosphorylation and aberrant DNA replication re-initiation. Furthermore, BRD4 inhibition sensitized cancer cells to various replication stress-inducing agents, and synergized with ATR inhibitor AZD6738 to induce cell killing across a number of cancer cell lines. The synergistic interaction between AZD5153 and AZD6738 is translatable to *in vivo* ovarian cell-line and patient-derived xenograft models. Taken together, our study uncovers a new biological function of BRD4 and provides mechanistic rationale for combining BET inhibitors with DDR-targeted agents for cancer therapy.

Keywords

BRD4; BET bromodomain inhibition; DNA damage response; replication stress; AZD5153; AZD6738

Introduction

During each round of cell cycle, 3×10^9 base pairs of genetic information needs to be precisely duplicated and distributed into daughter cells. Meanwhile, cells are constantly challenged by endogenous and exogenous insults that lead to errors during the DNA

Correspondence Huawei Chen, Oncology, IMED Biotech Unit, AstraZeneca, 35 Gatehouse Drive, Waltham, MA, 02451, USA, +1 781-839-4417, raymond.chen@astrazeneca.com.

Conflict of interest:

J.Z., A.M.D., M.H.H., B.S.W., J.N., A.W., A.L., C.R., M.Z., S.E.F., and H.C. are employees of AstraZeneca Pharmaceuticals LP, and G.B.M chairs the Scientific Advisory Board of IMED Oncology and receives sponsored research support from AstraZeneca.

replication process. Depletion of the nucleotide pool and disruption of chromatin structure can cause replication stress(1). In tumors, uncontrolled activation of oncogenes such as *RAS*, *MYC*, and *CCNE1* can lead to increased transcription and DNA replication origin firing, which have also been linked to elevated replication stress(1, 2). Under conditions of replication stress, the Minichromosome maintenance (MCM) replicative helicase complex becomes uncoupled from the DNA replication machinery, and single-stranded DNA (ssDNA) is generated as a result of continuous DNA unwinding(1, 3). Unprotected ssDNA triggers the activation of the replication stress response, also known as the intra-S phase checkpoint response. In this process, the ATR-CHK1 signaling axis plays a prominent role(3, 4). Activation of CHK1 and its downstream effectors lead to an array of coordinated activities that include reduced new origin firing, delay of cell cycle progression, and restoration of the stalled replication forks(3). In contrast, a defective intra-S phase checkpoint allows DNA replication and cell cycle progression in the presence of stalled replication forks and damaged DNA. Persistent replication stress will lead to replication fork collapse, DNA strand breaks, chromosome mis-segregation and genome instability(2, 5).

BET (bromodomain and extraterminal domain) family proteins, BRD2, BRD3, BRD4 and BRDT, are a family of epigenetic readers that recognize acetylated-lysine residues on histones and non-histone chromatin factors(6, 7). BRD4, the best studied member of this family, has been implicated in various human cancers(8–11). To date, a majority of BRD4 cancer dependency has been attributed to its role in regulating gene transcription through recruitment of transcription regulatory complexes, such as the general initiation cofactor Mediator and the Positive Transcription Elongation Factor b (pTEFb)(12–14). Recently, after the chemical feasibility of small molecule BET bromodomain inhibition was demonstrated, there has been intense interest in targeting BRD4 for cancer therapy. Several BET bromodomain inhibitors (BETi) capable of disrupting BET protein interactions with chromatin and other nuclear proteins have shown anti-tumor activity in a number of preclinical cancer models(6, 8). A subset of those BETi have demonstrated initial promising clinical activity in acute leukemia, lymphoma, and NUT midline carcinoma (NMC)(9, 15, 16).

Here, we explored unidentified BRD4 functions and describe a novel role of BRD4 in DNA replication stress response. We show that BRD4 associates with the DNA pre-replication complex and regulates its activity. Blockade of BRD4 function with BETi or siRNA-mediated BRD4 knockdown resulted in defective intra-S phase checkpoint signaling and sensitized cancer cells to both replication stress-inducing chemotherapy and a small molecule inhibitor of the ATR kinase, AZD6738.

Results

BRD4 associates with the DNA pre-replication complex and regulates DNA replication checkpoint signaling

To identify novel functions of BRD4, we examined BRD4-associated proteins under different growth conditions via immune-affinity purification and mass spectrometry (MS) analysis. 239 high-confidence protein targets that selectively interact with BRD4 compared to isotype control with Exponentially Modified Protein Abundance Index (emPAI) >0.1 were

identified in U2OS osteosarcoma cells (Table S1). These targets were further subjected to pathway and protein-complex based enrichment analysis (Figure 1A). Consistent with previous reports, proteins involved in regulating gene expression, cell cycle progression and mitosis were enriched (Figure 1A)(12, 13, 17, 18). Interestingly, several components of the DNA pre-replication complex, including CDC6, MCM5 and MCM7, were identified as high-confidence BRD4 interacting proteins (Figure 1B)(19). Among these pre-replication factors, CDC6 exhibited the most consistent and strongest interaction with BRD4 under all MS conditions evaluated (Table S1). We verified the association between BRD4 and CDC6, and similarly with another pre-replication complex member CDC7, by protein co-immunoprecipitation followed by western blot analysis in U2OS cells and OVCAR3 ovarian cancer cells. The consistent interactions between BRD4 and CDC6 observed in different cancer cell lines and under different cell lysis conditions (Benzonase and sonication) suggest that this interaction is broadly relevant (Figure 1C, Figure S1A). However, the interaction between BRD4 and the DNA pre-replication complex is not likely mediated through the BRD4 bromodomains as the potent BET bromodomain inhibitor AZD5153 did not disrupt their interactions (Figure 1C)(8, 20, 21).

BRD4 plays a role in regulating DNA replication checkpoint signaling

During DNA replication initiation, CDC6 functions as a replication licensing factor by binding to the origin recognition complex (ORC) and facilitates the assembly of the DNA pre-replication complex and recruitment of the DNA replication machinery(22). Additionally, CDC6 serves an important role in the activation and maintenance of the intra-S phase replication checkpoint response(19, 22). Association of BRD4 with CDC6 prompted us to investigate whether BRD4 has a function in these processes. To examine whether BRD4 modulates the DNA replication checkpoint response, we utilized AZD5153 to abrogate the function of BRD4 BET bromodomains and hydroxyurea (HU) to induce exogenous DNA replication stress(23). In U2OS cells, treatment with HU led to strong CHK1 activation as evidenced by marked increase of CHK1 phosphorylation at Ser317 (pCHK1 S317) (Figure 1D, left panel) as well as Ser345 (Figure S1B). Interestingly, the HU-induced CHK1 activation was significantly attenuated when cells were co-treated with AZD5153 over a time course of 2- to 6-hours, or when BRD4 protein expression was decreased by siRNA-mediated knockdown (Figure 1D, Figure S1B-C). The phosphorylation level of ATR (pATR T1989), an upstream kinase of CHK1 which senses RPA-coated single-stranded DNA generated upon uncoupling of replisomes and DNA unwinding(24), was not altered by either HU treatment or HU in combination with AZD5153 (Figure 1D). However, due to the limitation with the commercially available pATR antibody, we can’t be certain if the kinase activity of ATR is influenced by AZD5153. We next tested in an in vitro kinase assay and confirmed that AZD5153 or JQ1, two BETi with distinct chemical structures, do not inhibit ATR kinase activity (Figure S1D). Furthermore, no detectable modulation was observed for phospho-ATM (S1981) or downstream phospho-CHK2 (T68) (Figure 1D), two key proteins involved in DDR signaling during ATM-dependent DNA double-strand break repair(25). The increase of pCHK1 level induced by HU and the dampened effect exerted by BRD4 bromodomain inhibition were observed without a concomitant change in total protein or mRNA levels of CHK1, ATR activators TopBP1 and Rad17, or other DNA replication and DNA damage response factors (Figure S1E-F), and were not recapitulated by treatment with

general gene transcriptional inhibitors Flavopiridol or Dinaciclib (Figure S1G)(26, 27), suggesting that this is independent of the transcription regulatory activity of BRD4.

To confirm this mechanism in an alternative cellular context, we evaluated the effect of BETi on pCHK1 levels in OVCAR3 ovarian cancer cells. OVCAR3 cells harbor *CCNE1* amplification and exhibit high endogenous replication stress leading to elevated basal pCHK1 signaling activity (Figure 1E)(28). When OVCAR3 cells were treated with JQ1 or AZD5153, we observed a time-dependent reduction of pCHK1 seen as early as 30 min post treatment, with a maximal decrease in pCHK1(~80% reduction by JQ1 and >95% by AZD5153) reached at 1h and maintained throughout the duration of the experiment (Figure 1E). The modulation of pCHK1 by AZD5153 is also dose-dependent, with a potency that is comparable to the affinity of AZD5153 to BRD4 bromodomains (Figure 1F and Figure S1H). These findings demonstrate that BRD4 can regulate CHK1 signaling in response to both endogenous and exogenous DNA replication stress.

Inhibition of BRD4 leads to aberrant DNA replication re-initiation and sensitizes cells to replication stress-inducing agents

CHK1 activation following replication stress triggers an array of downstream signaling events, which lead to deceleration of ongoing replication, inhibition of new replication origin firing and recruitment of DNA repair machinery. In order to examine outcomes associated with defective intra-S phase checkpoint following BRD4 inhibition, we developed an imaging-based assay to monitor DNA replication activity in cultured cancer cells (Figure 2A). This assay utilized the dual pulse labeling with two nucleotide analogs, 5-bromo-2'-deoxyuridine (BrdU) and 5-Ethynyl-2'-deoxyuridine (EdU), to directly monitor the impact of BETi treatment on DNA replication activity following release from HU-induced DNA replication arrest. Consistent with expectations, DNA replication was completely blocked after HU treatment (Figure 2B, HU only). Four hours after HU was removed from the culture media, a baseline DNA replication activity, as indicated by EdU incorporation, resumed in DMSO-treated control cells (Figure 2B, DMSO). Remarkably, there was ~30% increase of EdU incorporation when cells were treated with JQ1 or AZD5153 (Figure 2B-C), a level that is comparable to ATR inhibitor AZD6738 (Figure S2A)(29, 30). These results suggest that BETi-induced defective intra-S phase checkpoint signaling can give rise to hyper-activated DNA replication following replication stress, possibly due to aberrant restart of stalled replication forks or firing of dormant origins. Consistent with previous findings, we were unable to recapitulate the same enhanced DNA replication phenotype with general transcription inhibitors Flavopiridol or Dinaciclib (Figure S2B).

We next assessed whether reduced CHK1 signaling caused by BET inhibition led to defective downstream G2/M checkpoint and increased sensitivity to replication stress-inducing agents. Indeed, cell treated with AZD5153 was able to circumvent the mitotic blockade under replication stress conditions induced by etoposide, similar to the effects exerted by an ATR kinase inhibitor (Figure S2C). Accumulation of DNA damage as indicated by γH2AX was measured by flow cytometry in U2OS cells treated with HU in the absence or presence of AZD5153. Continuous treatment of HU resulted in a time-dependent increase in the number of γH2AX positive cells (Figure 2D-E). When AZD5153 and HU

were added simultaneously, the number of γH2AX positive cells increased by more than 2 fold compared to HU treatment alone (Figure 2D-E). Interestingly, when AZD5153 was combined with etoposide, another replication stress-inducing agent with a different mode of action(31), we observed enhanced cell killing in a five day cell viability experiment (Figure S2D). This observation is consistent with the notion that BRD4 inhibition leads to defective replication stress checkpoint, which exacerbates the cytotoxicity effect of a DNA replication stress-inducing agent. Together, these data further support a role of BRD4 in mediating a proficient DNA replication stress response and point to potential therapeutic applications of BET inhibitors in tumors with high intrinsic replication stress or when combined with agents that induce DNA replication stress.

Defective replication stress response induced by BRD4 inhibition is CDC6 dependent

Previous reports demonstrated that CDC6 is required for the activation of replication checkpoint response(22). Therefore, we aimed to determine whether the BETi-induced defective S-phase checkpoint response is dependent on CDC6. When CDC6 protein was depleted by siRNA in U2OS cells, we observed a marked decrease in HU-induced CHK1 phosphorylation (Figure S3A). While there was a moderate decrease of the percentage of replicating cells and baseline DNA replication activity, CDC6 knockdowns clearly abrogated the enhanced DNA replication activity induced by BETi treatment, resulting in an EdU incorporation level that was comparable to DMSO control (Figure 3A, Figure S3B). To further establish that the role of BRD4 in intra-S phase checkpoint signaling is dependent on the CDC6 signaling pathway, two small molecule inhibitors XL413 and PHA767491, which target a CDC6 downstream effector kinase CDC7, were used in a set of analogous experiments (32, 33). We first confirmed the mechanism of action of these two compounds by monitoring the modulation of phospho-MCM2 S53 and S40/S41, two known CDC7 phosphorylation sites, and lack of modulation of phospho-MCM S108, a non-CDC7 phosphorylation site (Figure S3C). Consistently, CDC7 inhibition reduced baseline replication activity. CDC7 inhibitors treatment also abolished BETi-induced aberrant replication re-initiation, resulting in a reduction in DNA replication activity comparable to the effects seen with CDC6 protein knockdown (Figure 3B). Altogether, these data support that BET inhibitor treatment leads to aberrant DNA replication through a CDC6-dependent mechanism.

To further dissect the interplay between BRD4 and CDC6 signaling pathways, we examined the effect of BET inhibition on CDC6 function. During DNA replication licensing and pre-replication complex assembly, CDC6 activity is tightly regulated by cyclin-dependent kinases (CDKs)-mediated phosphorylation in a cell cycle-dependent fashion. CDK2 phosphorylates CDC6 at Ser54 during G1 phase, which serves as an activation signal to stimulate the recruitment of MCM complex and pre-replication complex assembly under normal growth conditions(34–36). This phosphorylation event has also been shown to regulate CDC6 localization and stability (36–38). Following a 2-hour AZD5153 treatment, we observed a significant increase in the percentage of cells stained positive for nuclear phospho-CDC6 (Ser54) foci, increasing from 33% in DMSO-treated group to 93% in AZD5153-treated group, and a ~14% increase in total nuclear phospho-CDC6 intensity (Figure 3C-D, Figure S3D). Cell cycle analysis revealed that AZD5153 treatment did not

alter cell cycle distribution, suggesting that changes in CDC6 phoshporylation is unlikely due to cell cycle blockade (Figure S3E). Next, we examined whether the increase in CDC6 phosphorylation status affects its stability. We used cycloheximide to block new protein synthesis and monitored both phospho-CDC6 Ser54 and total CDC6 turnover after AZD5153 treatment. Consistent with previous observation, AZD5153 caused an increase in phospho-CDC6 levels (Figure 3E, t=0). Interestingly, phospho-CDC6, and to a lesser degree total CDC6, degraded at a faster rate in the presence of AZD5153 (Figure 3E). These observations suggested that AZD5153 treatment causes an accumulation of active CDC6 on chromatin to promote hyper-activated DNA replication activity. However, the alteration in CDC6 activity also triggers faster turnover of CDC6, possibly leading to defective intra S-phase checkpoint signaling. Altogether, these data demonstrated that disruption of BRD4 function with BET inhibitor impacts CDC6 activity, and that CDC6 and BRD4 are both required for proficient DNA replication stress signaling.

BRD4 regulates CHK1 activation and combined inhibition of BRD4 and ATR results in enhanced DNA damage and apoptosis

As a central signaling molecule during intra-S phase checkpoint activation, CHK1 is predominantly activated by the upstream kinase ATR. However, CHK1 can also be activated through ATR-independent pathways(39, 40). Under conditions where BETi attenuated CHK1 activation in response to replication stress, we could not determine whether cellular ATR activity was modulated by AZD5153 due to technical limitations, but we have confirmed that neither AZD5153 or JQ1 inhibits ATR kinase activity *in vitro* (Figure S1D). We further investigated the relationship between BETi-regulated CHK1 signaling and the ATR-CHK1 signaling axis by examining the effects of combined inhibition of ATR (with AZD6738) and BRD4 (with JQ1 or AZD5153) in OVCAR3 cells. Relatively low concentrations of AZD6738 or BETi (JQ1 or AZD5153) were chosen as each agent on its own only results in partial inhibition of pCHK1. When AZD6738 was combined with either JQ1 or AZD5153, near complete inhibition of pCHK1 was achieved (Figure 4A). This result suggests a specific mechanism where either BRD4 and ATR function in non-overlapping pathways in regulating CHK1 signaling activity, or BRD4 indirectly regulates ATR/CHK1 signaling pathway through other regulatory components. Yet, a clearly combination benefit was seen with concurrent ATR kinase activity inhibition (with AZD6738) and BRD4 inhibition.

We hypothesized that combination of BET and ATR inhibitors may lead to a compound defect in DNA replication checkpoint response and synergy in inducing DNA damage and cell death. To test this hypothesis, we assessed the DNA damage levels following co-treatment with BRD4 and ATR inhibitors in OVCAR3 ovarian cancer cells. Consistent with their respective role in replication stress response signaling, single agent treatment with AZD5153 or AZD6738 caused an accumulation of DNA damage marker, γH2AX, in a time-dependent manner (Figure 4B-C). Notably, combination treatment of AZD5153 and AZD6738 caused an increase of accumulated γH2AX that is enriched in S-phase cells (Figure 4B-D). Moreover, the synergistic induction of DNA damage and apoptosis was observed across several cancer cell lines (Figure 4E). Next, we expanded our study to a cancer cell line panel consisting of 67 lines spanning five different cancer types. When we

examined the combination activity of AZD5153 and AZD6738 in this panel, we observed striking synergistic cell killing in a significant fraction of tested cell lines. However, when AZD5153 was combined with an ATM inhibitor (41), the synergy was largely absent (Figure 4F, Table S2). These findings are consistent with the mechanistic interaction we depicted, and further reinforce the notion that there is specific mechanistic foundation for the combination benefit between BRD4 and ATR inhibitors.

Next we examined if the combination of BRD4 and ATR inhibition could be extended to the *in vivo* setting. AZD5153 and AZD6738 were administered either as single agent or in combination to OVCAR3 tumor-bearing mice. AZD5153 or AZD6738 single agent treatment, as well as co-administration of both drugs, were well tolerated, and no significant body weight loss was observed in treated animals (Figure 5A). After three weeks of dosing, co-administration of AZD5153 and AZD6738 significantly inhibited tumor growth relative to each single agent alone (tumor growth inhibition after 21 day dosing: AZD6738, 58%; AZD5153, 74%; combo, >100% TGI with 21% tumor regression, $p<0.0001$) (Figures 5A and S4A). Pharmacodynamics study revealed that increased levels of single-stranded DNA, DNA damage and apoptosis, indicated by phospho-RPA, γH2AX and cleaved-PARP respectively, were observed in tumor samples following repeated co-treatment with AZD5153 and AZD6738 (Figure 5B). To further evaluate the *in vivo* efficacy of combined inhibition of ATR and BRD4, we tested this concept in three ovarian patient-derived xenograft (PDX) models utilizing a mouse clinical trial format, where three tumor-bearing mice were included in the vehicle group to account for variability in tumor growth and a single tumor-bearing mouse was enrolled onto each treatment group. Compared to either single agent alone, the combination of AZD5153 and AZD6738 exhibited significantly stronger anti-tumor activity in two of the three PDX models (GTG-0258 and CTG-0486) (Figures 5C and S4B). These data suggest that, due to the parallel nature of ATR and BRD4 in regulating CHK1 activation, combined inhibition of ATR and BRD4 can potentially afford greater anti-tumor efficacy *in vivo* by synergistically inducing DNA damage and apoptosis.

Discussion

In this study, we describe a novel function for the BET epigenetic reader protein, BRD4, in DNA damage response signaling. Specifically, we demonstrate that BRD4 is an important signaling molecule for intra-S phase replication checkpoint activation. Small molecule-mediated inhibition and siRNA-mediated knockdown of BRD4 lead to defective CHK1 activation in response to exogenous and endogenous replication stress. In contrast to the well-established role of BRD4 in transcription regulation, we provide evidence that BRD4 regulates DNA damage response signaling in a transcriptionally-independent manner. First line of evidence that supports this statement is that defective CHK1 signaling was not accompanied by changes in the expression levels of key relevant signaling factors following BET inhibition. Secondly, the aberrant replication phenotype induced by AZD5153 treatment cannot be recapitulated by pan-transcription inhibitors treatment. Mechanistic studies reveal that BRD4 modulates the activity of CDC6, a component of the DNA pre-replication complex that has been implicated in replication stress response signaling. BETi treatment leads to activation and faster turnover of CDC6, and enhanced replication re-

initiation following replication stress challenge. As a result, BETi treatment sensitizes cancer cells to replication stress-inducing agents such as HU or etoposide.

The prominent role of BRD4 in modulating replication stress response signaling could be envisaged, as dynamic epigenetic modifications at, or near, sites of DNA damage are crucial for proper initiation of DNA damage response signaling, particularly in the case of DNA double-strand break (DSB) repair(42). It has been estimated that over a third of human bromodomain containing proteins respond to DNA damage, either directly by locating to DNA damage sites or indirectly by affecting chromatin structures near damage sites(43). Previous studies showed that BRD4 associates with chromatin near replication forks, BRD4 can function as a repair complex adaptor in nonhomologous end joining, and can also suppress DNA double strand break signaling by regulating chromatin condensation(18, 44, 45). We hypothesize that BRD4-chromatin association is required for maintaining an unperturbed replication stress response signaling. Although AZD5153 treatment had no impact on the interaction between CDC6 and BRD4, we suspect that BRD4 displacement from chromatin may perturb the recruitment or redistribution of regulatory factors in response to replication stress, resulting in the immobilization of CDC6 to specific chromatin locations and its activation and turnover. Future studies warrant a more detailed mechanistic evaluation of how BRD4 recognizes chromatin near stalled replication forks and how BRD4 regulates CDC6 activation.

Targeting the DDR pathways is a promising therapeutic strategy in treating cancers that are defective in one or more of the DDR pathways or show increased dependency on DDR due to elevated DNA damage levels(46, 47). One good example is the recent approval of olaparib (Lynparza™), a poly ADP-ribose polymerase (PARP) inhibitor, in treating ovarian cancers which harbor *BRCA1* or *BRCA2* mutations(48, 49). In a similar fashion, ATR and CHK1 inhibitors have been shown to cause selective cytotoxic effects in cancer cells over-expressing *CCNE1*, due to their increased dependency on ATR/CHK1 signaling to cope with CyclinE1-induced replication stress(50). Interestingly, BRD4 is focally amplified in ~18% HGSOC samples (TCGA), and often is co-amplified with *CCNE1* as they are both located near the centromere of chromosome 19. These copy-number alterations are also mutually-exclusive with *BRCA1* and *BRCA2* loss-of-function mutations(51). We showed that BRD4 regulates CHK1 activation through a mechanism that is likely to be independent of ATR signaling, and concurrent treatment with BETi and ATRi leads to a more profound inhibition of CHK1 activity, increase of DNA damage, and enhanced anti-cancer effects in a range of *in vitro* and *in vivo* models. These findings demonstrate promise of BRD4-targeted agents as a therapeutic option in ovarian cancers, particularly in the non-BRCA1/2 mutant population that exhibit high replication stress. Further investigation is needed to explore the combination of BETi with other DDR-targeted agents in treating cancer types that exhibit specific DDR dependencies.

In conclusion, we uncovered a key role of BRD4 in mediating replication stress response signaling and expanded our understanding of the physiological functions of BET proteins. Combining BETi with specific DDR-targeted agents may offer superior efficacy in tumors with high replication stress or those exhibiting increased dependency on CHK1-mediated checkpoint activity. Together with previously described role of BRD4 in transcription

regulation, we propose that BET inhibitors may exert anti-tumor effects through multiple mechanisms, i.e. preventing transcription of key oncogenic programs and exacerbating replication stress responses.

Material and Methods

Cells and reagents:

U2OS and OVCAR3 cells were purchased from ATCC. Antibodies used for Western Blot analysis were from Cell Signaling (Danvers, MA, USA): CDC6 (CS3387), CDK9 (CS2316), phospho-CHK1 Ser317 (CS12302), phospho-CHK1 Ser345 (CS2348), CHK1 (CS2360), phospho-CHK2 Thr68 (CS2197), CHK2 (CS6334), ATR (CS2790), ATRIP (CS2737), Claspin (CS2800), Germinin (CS5165), phospho-ATM Ser1981 (CS5883), CDT1 (CS8064), cleaved caspase 3 Asp175 (CS9661), MRE11 (CS4847), NBS1 (CS14956), Rad17 (CS8561), TOPBP1 (CS14342), MCM2 (CS3619), cleaved-PARP Asp214 (CS5625), RPA (CS2208), GAPDH (CS5174), Histone H3 (CS4499); from Bethyl Laboratories (Montgomery, TX, USA): CDC7 (A302–504A), phospho-RPA32 S4/S8 (A300–245A), phospho-RPA32 S33 (A300246A), phospho-MCM2 S108 (A300–094A), phospho-MCM2 S53 (A300–756A), phospho-MCM2 S40/41 (A300–788A); from Millipore: phospho-Histone H2A.X Ser139 (05–636); from Abcam (Cambridge, MA, USA): BRD4 (ab128874), phospho-CDC6 Ser54 (ab75809), ETAA1 (ab197017); from Genetex (Irvine, CA, USA): phospho ATR-Thr1989 (GTX128145); from Sigma (St. Louis, MO, USA): vinculin (V9264); and from Covance (Dedham, MA, USA): Phospho-RNA Pol II Ser2 (#MMS-129R). Reagents were purchased from Sigma (St. Louis, MO, USA): Hydroxyurea (H8627), BrdU (B5002); from Selleckchem: JQ1 (S7110), Flavopiridol (S1230), Dinaciclib (S2768), etoposide (S1225), XL413 (S7547), PHA-767491 (S2742). AZD5153, AZD6738 and ATM inhibitor compound 72 were developed by AstraZeneca.

Western Blot analysis:

After treatment, cells were lysed in cell lysis buffer (25mM Tris7.4, 300mM NaCl, 1mM EDTA, 1% Triton) supplemented with protease and phosphatase inhibitor cocktail (Cell Signaling #5872). For xenograft tumor samples, tissues were homogenized in SDS lysis buffer (100mM Tris-HCl buffer, pH7.4, 10% Glycerol and 1% SDS) supplemented with protease and phosphatase inhibitor cocktail. 4μg of lysates were loaded for immunoblotting following standard procedures. For protein halflife studies, U2OS cells were first treated with DMSO or AZD5153 for 30 minutes before addition of 10 μg/ml of cycloheximide (Cell Signaling #2112). Cell extracts were collected after various amounts of time, and the expression levels of proteins of interest were examined by western blot analysis following standard procedure.

Immunofluorescence:

After AZD5153 treatment, U2OS cells were pre-extracted with 0.5% triton in PBS for 5 min before being fixed with 4% paraformaldehyde for 15 min at room temperature. Cells were then blocked with 5% BSA in PBST followed by primary antibody (Phospho-CDC6 S54, Abcam # ab75809, 1:500) and secondary antibody (Alexa Fluor 488 conjugate) staining. DAPI was used to counter stain DNA. Image acquisition was carried out on ImageXpress

MicroXL High Content Screening System (Molecular Devices, Sunnyvale, CA, USA). The number of phospho-CDC6 foci in the nuclei was scored and quantified using MetaXpress Software (Molecular Devices). An average of 500 nuclei were analyzed for each experimental condition. Results shown represent average of three independent experiments.

Replication re-initiation/restart assay and quantification:

U2OS cells were first pulse-labeled with 10μM BrdU for 30 min followed by 2X PBS wash and then treated with 2mM HU in growth medium for 1 hour. Next, cells were washed twice with PBS and replenished with fresh growth media containing different inhibitors. After a 4h recovery in fresh media with the presence of different inhibitors, cells were pulse-labeled with 10μM EdU for 30 min before being fixed for staining. For BrdU and EdU staining, cells were fixed with 4% paraformaldehyde for 15 min at RT. After 2X PBS wash, DNA were denatured with 2N HCl in PBS for 20 min at RT followed by 2X wash with PBS. Cell were then permeabilized with 0.5% Triton in PBS for 5 min at RT and blocked with 5% BSA in PBST for 30 min at RT. Click-iT® Plus EdU Alexa Fluor® 647 Imaging Kit (#C10340, Thermo Fisher Scientific, Waltham, MA, USA) was used to stain EdU following manufacturer's protocol. After EdU staining, cells were incubated with anti-BrdU antibody (Cell Signaling #CS5292, 1:500) for 3h at RT before secondary antibody (Alexa Fluor 488 conjugate) and DAPI staining. Image acquisition was carried out on ImageXpress MicroXL High Content Screening System (Molecular Devices). EdU intensity was scored in BrdU positive cells and data analysis was performed with MetaXpress Software (Molecular Devices). Results shown represent average of three independent experiments. Statistical significance was evaluated using two-tailed t test.

Flow cytometry and cell cycle analysis:

For cell cycle analysis, treated cells were labeled with 10μM EdU for 1 hour before being fixed and stained for EdU and DNA content using Click-iT™ Plus EdU Alexa Fluor™ 647 Flow Cytometry Assay Kit (C10634, Thermo Fisher Scientific, Waltham, MA) following manufacturer's instructions. For measuring cellular γH2AX levels, treated cells were trypsinized from cell culture plates and fixed with 4% paraformaldehyde. 1×10^6 cells were washed once with 1 % BSA-PBS and permeabilized with 0.2% Trition in PBS for 15 minutes at RT. FITC-conjugated γH2AX antibody (#06–202A, Millipore, Bellerica, MA, USA) was added to cells and allowed to stain for 1 hour at RT in the dark. Cells were then washed once with 1 % BSA-PBS and resuspended in 200 μl PBS containing DAPI (final concentration 1μg/μl). After 30 min incubation in the dark, samples were analyzed on a LSRFortessa cytometer (BD, San Jose, CA, USA). For G2/M checkpoint analysis, PE-conjugated phospho-Histone H3 Ser10 antibody (#5764, Cell Signaling) was used to stain havested cells after 24 hour treatment with 10μM Etoposide following the same staining procedure. Data analysis was done with FlowJo V7.0. For each experiment, 150,000 events were captured and analyzed. Results shown represent average of three independent experiments.

Immunoprecipitation, Mass Spec and data analysis

For immunoprecipitation, 5×10^6 U2OS cells were resuspended in lysis buffer (50mM Tris 7.4, 150mM NaCl, 1mM EDTA, 0.5% NP-40) supplemented with protease and phosphatase

inhibitors. Cell lysates were then processed in two different ways. For benzonase treatment, 25 U/ml final concentration of benzonase (E1014, Sigma) was added to the lysates and incubated on ice for 30 minutes to digest chromatins. For benzonase-free lysis condition, cell lysates were then sonicated on a bioruptor (Diagenode, Denville, NJ, USA) for 6 cycles (30s on, 60s off) on medium setting. After sonication or benzonase treatment, cell lysates were cleared by centrifugation and then pre-cleared with protein A magnetic beads (Life Technologies #10002D). BRD4 antibody (Abcam #128874) was conjugated to protein A magnetic beads using 2mM BS reagent (Thermo Fisher #21585) in conjugation buffer (30mM Sodium Phosphate, 0.15M NaCl) for 30 min at RT. Conjugation reaction was stopped by quenching the reaction with 1M Tris HCl (PH 7.5, 50mM final concentration). Pre-cleared lysates and BRD4 antibody-conjugated protein A beads were then incubated together at 4 °C overnight with agitation. The next day, beads were washed 4 times with lysis buffer before sample buffer was added to elute the immuno-complexes.

For Mass Spec analysis, 2×10^7 U2OS cells were used for BRD4 pull-down following the same immunoprecipitation protocol. After overnight incubation, beads were washed 2X with lysis buffer, 2X with PBST and 2X with PBS. Washed beads were then resuspended in 50 µl 8M Urea/300mM NH_4HCO_3. 5 µL 45mM DTT was added to each sample followed by incubation at 37 °C for 30 min with shaking. After the reaction mix cooled down to RT, 5 µl 100mM Iodozcetamide was added and incubated for 30 min at RT in the dark. Next, the volume of beads mixture was brought up to 200 µl with water for overnight trypsin digestion. Trypsin (0.5 µg/µl working concentration) was added and the reaction mixture was incubated overnight at 37 °C with shaking. The next day, solution digests were desalted with C18 columns (ThermoFisher #89873) following standard protocols. Elution was vacuum dried and frozen down. Mass Spectrometry analysis was performed by the proteomics facility at the Keck Biotechnology Resource Laboratory at Yale University (http://medicine.yale.edu/keck/proteomics/index.aspx). Mascot software was used to identify proteins from LC-MS/MS data against the Swiss-Prot human database using a 1% false discovery rate (FDR).

Cell viability assay and combination screening:

For cancer cell line panel screening, detailed experimental procedure and data analysis have been previously described(52). Briefly, optimal 384-well seeding densities were pre-determined for linear growth over 5 days. Cell suspension (30 µl per well) was seeded into 384-well plates. Cells were allowed to grow overnight, and then treated with increasing concentrations of compounds in a 6×6 dosing matrix using Echo automatic dosing (Labcyte, San Jose, CA). After 5 days of growth, cell viability was measured using using an Alamar Blue (Invitrogen #DAL1100) or Sytox Green (Invitrogen S7020) endpoint following manufacturer's protocol. Pre-dose measurements were made to indicate the number of live cells at the start of the experiment and thus an indication of whether the treatment regimen had resulted in cell death. The data are presented as % growth using the NCI formulas as follows: [(Ti-Tz)/(C-Tz)] ×100 for values for which Ti≥Tz, and [(Ti-Tz)/Tz] ×100 for concentrations for which Ti<Tz (Tz represents the number of live cells at time zero, C represents the control growth and Ti represents the number of live cells in the presence of each drug regimen). This formula gives a growth percentage from −100% to +100%.

Negative scores are for cell killing and positive scores are for anti-proliferation. Experiments were performed in triplicate.

Two dimensional dose response matrix and curve fitting were processed in the combination extension of Genedata Screener12™ (Genedata, Basel, Switzerland). To enable this, % growth values were converted to a positive scale using a modified NCI formula as follows: [1-(Ti-Tz)/(C-Tz)] ×100 for values for which Ti≥Tz, and [1-(Ti-Tz)/Tz] ×100 for concentrations for which Ti<Tz. This gave a scale of 0–200% growth inhibition where 0–100% is for anti-proliferation and 100–200% is for cell killing. Combination activity (synergism) was calculated using the Loewe dose-additivity model as previously described (53). This model of additivity provides a null-reference that is predicted by the expected response if the two agents were the same drug. The 3-dimensional model surface, predicted from the two single-agent response curves, is subtracted from the experimentally-derived 3-dimensional dose effect surface to generate a difference volume. This excess matrix volume can be integrated to generate a synergy score.

Quantitative PCR:

Taqman Gene Expression assays were purchased from ThermoFisher Scientific (Waltham, MA, USA): *ATR* (Hs00992123_m1), *ATRIP* (Hs04335019_s1), *CDC6* (HS00154374_m1), *CDT1* (Hs00925491_g1), *CHEK1*/CHK1 (Hs00967506_m1), *CHEK2*/CHK2 (Hs00200485_m1), *CLSPN*/Claspin (Hs00898637_m1), *ETAA1*(Hs00936568_m1), *GMNN*/Geminin (Hs00992846_m1), *MRE11A* (Hs00967437_m1), *NBN*/NBS1(Hs01039845_m1), *RAD17* (Hs00607830_m1), *RPA2* (Hs00989573_g1), *TOPBP1* (Hs00199775_m1), *GAPDH* (Hs02786624_g1). qPCR reactions were carried out on a 7500 HT instrument (Applied biosystems, Foster City, CA, USA). The amplified transcript level of each specific gene was normalized to that of GAPDH. Results shown represent average of three independent experiments.

In vivo Efficacy and Pharmacodynamics (PD) Studies

Female C.B.−17 *scid* mice were purchased from Charles River Laboratories (Wilmington, MA). Mice were housed under pathogen-free conditions in individual ventilated cages (IVC) at our AAALAC (Association for the Assessment and Accreditation of Laboratory Animal Care) accredited facility in Waltham, MA. All animal manipulations were conducted in a biosafety cabinet maintained under positive pressure. Mice used were 5–6 weeks old at the time of tumor implantation. All animal studies were conducted in accordance with the guidelines established by the internal IACUC (Institutional Animal Care and Use Committee) and reported following the ARRIVE (Animal Research: Reporting In Vivo experiments) guidelines(54).

2×10^7 OVCAR3 tumor cells were injected subcutaneously in the right flank of the mice. Tumor volumes (measured by caliper), animal body weight, and tumor condition were recorded twice weekly for the duration of the study. The tumor volume was calculated (taking length to be the longest diameter across the tumor and width to be the corresponding perpendicular diameter) using the formula: length (mm) × width $(mm)^2/0.52$. For efficacy studies, tumor growth inhibition (TGI) was calculated as $(RTV_{control} - RTV_{treatment})*100)/$

($RTV_{control}$ − 1), where $RTV_{control}$ is the geometric mean of relative tumor volume of control group and $RTV_{treatment}$ is the treatment group. Data were log transformed to remove any size dependency before statistical evaluation. Statistical significance was evaluated using a one-tailed, 2-sample t test. For all studies, mice were randomized based on tumor volumes using stratified sampling and enrolled into control and treatment groups. For efficacy studies, dosing began when mean tumor size reached approximately 125 $mm^3$and for PD studies the average tumor volume at the time of dosing was 400 mm^3. Tumor samples for PD analysis were collected after four days of dosing.

PDX model screening was performed at Champions Oncology. Tumor fragments (2 mm^3) were implanted into the left flank of female mice (Nu/Nu, Harlan). Once the tumor volume reached an average of 200 mm^3, tumor volume was measured and mice were randomized into groups based on tumor volume. AZD5153, AZD6738 or the combination of the two drugs were dosed for 28 days and tumor volume and body weight were measured throughout the treatment period. Tumor growth inhibition was calculated based on changes in tumor volume on the last day that vehicle animals were available.

siRNA-mediated protein knockdown

Where indicated, cells were transfected with 25 pmol siRNA against CDC6 (Dharmacon J-003233–10, J-003233–12, J-003233–13, or L-003233 (pooled)), against BRD4 (Dharmacon J004937–06, J004937–07, J004937–08), or siRNA negative control (Invitrogen AM4611) using Lipofectamine RNAiMAX (Invitrogen 13778075) according to the manufacturer's instructions. Two days after siRNA transfection, cells were treated with HU for different periods of time and harvested for western blot analysis. For DNA replication re-initiation/restart assay, siRNA-transfected cells were split into 96-well plates one day after siRNA transfection for subsequent labeling and imaging analysis.

In vitro ATR kinase assay

In vitro ATR kinase assay was perforem by Eurofins Pharma Discovery Services (Dundee, UK). Briefly, ATR/ATRIP (human) is incubated in assay buffer containing 50 nM GST-cMyc-p53 and various concentrations of compounds. The reaction is initiated by the addition of the Mg/ATP (10 μM) mix. After incubation for 30 minutes at room temperature, the reaction is stopped by the addition of stop solution containing EDTA. Finally, detection buffer is added, which contains d2-labelled anti-GST monoclonal antibody, and a Europium-labelled anti-phospho Ser15 antibody against phosphorylated p53. The plate is then read in time-resolved fluorescence mode and the homogeneous time-resolved fluorescence (HTRF) signal is determined according to the formula HTRF = 10000 × (Em_{665nm}/Em_{620nm}). Results shown represent average of three independent experiments.

Supplementary Material

Refer to Web version on PubMed Central for supplementary material.

Acknowledgements:

We thank the W.M. Keck Biotechnology Resource Laboratory at Yale University School of Medicine for their mass spectrometry and proteomics service and technical support, Champions Oncology for performing patient-drived xenograft model screening, Eric Tang from AstraZeneca cell screening team for generating cell panel combination data, and Laura Prickett from Oncology Bioscience team for assistance with flow cytometry analysis. We would also like to thank team members of the AstraZeneca IMED Oncology DNA Damage Response Biology Area for critical reading of the manuscript and their expertise and suggestions.

References:

1. Zeman MK, Cimprich KA. Causes and consequences of replication stress. Nature cell biology. 2014;16(1):2–9. [PubMed: 24366029]
2. Dobbelstein M, Sorensen CS. Exploiting replicative stress to treat cancer. Nature reviews Drug discovery. 2015;14(6):405–23. [PubMed: 25953507]
3. O'Connor MJ. Targeting the DNA Damage Response in Cancer. Molecular cell. 2015;60(4):547–60. [PubMed: 26590714]
4. Zhou BB, Bartek J. Targeting the checkpoint kinases: chemosensitization versus chemoprotection. Nature reviews Cancer. 2004;4(3):216–25. [PubMed: 14993903]
5. Gelot C, Magdalou I, Lopez BS. Replication stress in Mammalian cells and its consequences for mitosis. Genes. 2015;6(2):267–98. [PubMed: 26010955]
6. Shi J, Vakoc CR. The mechanisms behind the therapeutic activity of BET bromodomain inhibition. Molecular cell. 2014;54(5):728–36. [PubMed: 24905006]
7. Chiang CM. Brd4 engagement from chromatin targeting to transcriptional regulation: selective contact with acetylated histone H3 and H4. F1000 biology reports. 2009;1:98. [PubMed: 20495683]
8. Rhyasen GW, Hattersley M, Yao Y, Dulak A, Wang W, Petteruti P, et al. AZD5153: a novel bivalent BET bromodomain inhibitor highly active against hematologic malignancies. Molecular cancer therapeutics. 2016.
9. Stathis A, Zucca E, Bekradda M, Gomez-Roca C, Delord JP, de La Motte Rouge T, et al. Clinical Response of Carcinomas Harboring the BRD4-NUT Oncoprotein to the Targeted Bromodomain Inhibitor OTX015/MK-8628. Cancer discovery. 2016;6(5):492–500. [PubMed: 26976114]
10. Baratta MG, Schinzel AC, Zwang Y, Bandopadhayay P, Bowman-Colin C, Kutt J, et al. An in-tumor genetic screen reveals that the BET bromodomain protein, BRD4, is a potential therapeutic target in ovarian carcinoma. Proceedings of the National Academy of Sciences of the United States of America. 2015;112(1):232–7. [PubMed: 25535366]
11. Zuber J, Shi J, Wang E, Rappaport AR, Herrmann H, Sison EA, et al. RNAi screen identifies Brd4 as a therapeutic target in acute myeloid leukaemia. Nature. 2011;478(7370):524–8. [PubMed: 21814200]
12. Jang MK, Mochizuki K, Zhou M, Jeong HS, Brady JN, Ozato K. The bromodomain protein Brd4 is a positive regulatory component of P-TEFb and stimulates RNA polymerase II-dependent transcription. Molecular cell. 2005;19(4):523–34. [PubMed: 16109376]
13. Yang Z, He N, Zhou Q. Brd4 recruits P-TEFb to chromosomes at late mitosis to promote G1 gene expression and cell cycle progression. Molecular and cellular biology. 2008;28(3):967–76. [PubMed: 18039861]
14. Wu SY, Chiang CM. The double bromodomain-containing chromatin adaptor Brd4 and transcriptional regulation. The Journal of biological chemistry. 2007;282(18):13141–5. [PubMed: 17329240]
15. Berthon C, Raffoux E, Thomas X, Vey N, Gomez-Roca C, Yee K, et al. Bromodomain inhibitor OTX015 in patients with acute leukaemia: a dose-escalation, phase 1 study. The Lancet Haematology. 2016;3(4):e186–95. [PubMed: 27063977]
16. Amorim S, Stathis A, Gleeson M, Iyengar S, Magarotto V, Leleu X, et al. Bromodomain inhibitor OTX015 in patients with lymphoma or multiple myeloma: a dose-escalation, open-label, pharmacokinetic, phase 1 study. The Lancet Haematology. 2016;3(4):e196–204. [PubMed: 27063978]

17. Dey A, Chitsaz F, Abbasi A, Misteli T, Ozato K. The double bromodomain protein Brd4 binds to acetylated chromatin during interphase and mitosis. Proceedings of the National Academy of Sciences of the United States of America. 2003;100(15):8758–63. [PubMed: 12840145]
18. Maruyama T, Farina A, Dey A, Cheong J, Bermudez VP, Tamura T, et al. A Mammalian bromodomain protein, brd4, interacts with replication factor C and inhibits progression to S phase. Molecular and cellular biology. 2002;22(18):6509–20. [PubMed: 12192049]
19. Borlado LR, Mendez J. CDC6: from DNA replication to cell cycle checkpoints and oncogenesis. Carcinogenesis. 2008;29(2):237–43. [PubMed: 18048387]
20. Bradbury RH, Callis R, Carr GR, Chen H, Clark E, Feron L, et al. Optimization of a Series of Bivalent Triazolopyridazine Based Bromodomain and Extraterminal Inhibitors: The Discovery of (3R)-4-[2-[4-[1-(3-Methoxy-[1,2,4]triazolo[4,3-b]pyridazin-6-yl)-4-piperidyl]phen oxy]ethyl]-1,3-dimethyl-piperazin-2-one (AZD5153). Journal of medicinal chemistry. 2016;59(17):7801–17. [PubMed: 27528113]
21. Waring MJ, Chen H, Rabow AA, Walker G, Bobby R, Boiko S, et al. Potent and selective bivalent inhibitors of BET bromodomains. Nature chemical biology. 2016.
22. Oehlmann M, Score AJ, Blow JJ. The role of Cdc6 in ensuring complete genome licensing and S phase checkpoint activation. The Journal of cell biology. 2004;165(2):181–90. [PubMed: 15096526]
23. Zhao H, Piwnica-Worms H. ATR-mediated checkpoint pathways regulate phosphorylation and activation of human Chk1. Molecular and cellular biology. 2001;21(13):4129–39. [PubMed: 11390642]
24. Nam EA, Zhao R, Glick GG, Bansbach CE, Friedman DB, Cortez D. Thr-1989 phosphorylation is a marker of active ataxia telangiectasia-mutated and Rad3-related (ATR) kinase. The Journal of biological chemistry. 2011;286(33):28707–14. [PubMed: 21705319]
25. Lee JH, Paull TT. ATM activation by DNA double-strand breaks through the Mre11-Rad50-Nbs1 complex. Science. 2005;308(5721):551–4. [PubMed: 15790808]
26. Baker A, Gregory GP, Verbrugge I, Kats L, Hilton JJ, Vidacs E, et al. The CDK9 Inhibitor Dinaciclib Exerts Potent Apoptotic and Antitumor Effects in Preclinical Models of MLL-Rearranged Acute Myeloid Leukemia. Cancer research. 2016;76(5):1158–69. [PubMed: 26627013]
27. Chen R, Keating MJ, Gandhi V, Plunkett W. Transcription inhibition by flavopiridol: mechanism of chronic lymphocytic leukemia cell death. Blood. 2005;106(7):2513–9. [PubMed: 15972445]
28. Etemadmoghadam D, Au-Yeung G, Wall M, Mitchell C, Kansara M, Loehrer E, et al. Resistance to CDK2 inhibitors is associated with selection of polyploid cells in CCNE1-amplified ovarian cancer. Clinical cancer research : an official journal of the American Association for Cancer Research. 2013;19(21):5960–71.
29. Foote KM, Lau A, Nissink JW. Drugging ATR: progress in the development of specific inhibitors for the treatment of cancer. Future medicinal chemistry. 2015;7(7):873–91. [PubMed: 26061106]
30. Vendetti FP, Lau A, Schamus S, Conrads TP, O'Connor MJ, Bakkenist CJ. The orally active and bioavailable ATR kinase inhibitor AZD6738 potentiates the anti-tumor effects of cisplatin to resolve ATM-deficient non-small cell lung cancer in vivo. Oncotarget. 2015;6(42):44289–305. [PubMed: 26517239]
31. Montecucco A, Biamonti G. Cellular response to etoposide treatment. Cancer letters. 2007;252(1): 9–18. [PubMed: 17166655]
32. Montagnoli A, Valsasina B, Croci V, Menichincheri M, Rainoldi S, Marchesi V, et al. A Cdc7 kinase inhibitor restricts initiation of DNA replication and has antitumor activity. Nature chemical biology. 2008;4(6):357–65. [PubMed: 18469809]
33. Koltun ES, Tsuhako AL, Brown DS, Aay N, Arcalas A, Chan V, et al. Discovery of XL413, a potent and selective CDC7 inhibitor. Bioorganic & medicinal chemistry letters. 2012;22(11):3727–31. [PubMed: 22560567]
34. Jiang W, Wells NJ, Hunter T. Multistep regulation of DNA replication by Cdk phosphorylation of HsCdc6. Proceedings of the National Academy of Sciences of the United States of America. 1999;96(11):6193–8. [PubMed: 10339564]

35. Duursma AM, Agami R. CDK-dependent stabilization of Cdc6: linking growth and stress signals to activation of DNA replication. Cell cycle. 2005;4(12):1725–8. [PubMed: 16258286]
36. Mailand N, Diffley JF. CDKs promote DNA replication origin licensing in human cells by protecting Cdc6 from APC/C-dependent proteolysis. Cell. 2005;122(6):915–26. [PubMed: 16153703]
37. Walter D, Hoffmann S, Komseli ES, Rappsilber J, Gorgoulis V, Sorensen CS. SCF(Cyclin F)-dependent degradation of CDC6 suppresses DNA re-replication. Nature communications. 2016;7:10530.
38. Elsasser S, Chi Y, Yang P, Campbell JL. Phosphorylation controls timing of Cdc6p destruction: A biochemical analysis. Molecular biology of the cell. 1999;10(10):3263–77. [PubMed: 10512865]
39. Chen Y, Caldwell JM, Pereira E, Baker RW, Sanchez Y. ATRMec1 phosphorylation-independent activation of Chk1 in vivo. The Journal of biological chemistry. 2009;284(1):182–90. [PubMed: 18984588]
40. Rodriguez-Bravo V, Guaita-Esteruelas S, Florensa R, Bachs O, Agell N. Chk1- and claspin-dependent but ATR/ATM- and Rad17-independent DNA replication checkpoint response in HeLa cells. Cancer research. 2006;66(17):8672–9. [PubMed: 16951182]
41. Degorce SL, Barlaam B, Cadogan E, Dishington A, Ducray R, Glossop SC, et al. Discovery of Novel 3-Quinoline Carboxamides as Potent, Selective, and Orally Bioavailable Inhibitors of Ataxia Telangiectasia Mutated (ATM) Kinase. Journal of medicinal chemistry. 2016;59(13):6281–92. [PubMed: 27259031]
42. Price BD, D'Andrea AD. Chromatin remodeling at DNA double-strand breaks. Cell. 2013;152(6):1344–54. [PubMed: 23498941]
43. Gong F, Chiu LY, Miller KM. Acetylation Reader Proteins: Linking Acetylation Signaling to Genome Maintenance and Cancer. PLoS genetics. 2016;12(9):e1006272. [PubMed: 27631103]
44. Stanlie A, Yousif AS, Akiyama H, Honjo T, Begum NA. Chromatin reader Brd4 functions in Ig class switching as a repair complex adaptor of nonhomologous end-joining. Molecular cell. 2014;55(1):97–110. [PubMed: 24954901]
45. Floyd SR, Pacold ME, Huang Q, Clarke SM, Lam FC, Cannell IG, et al. The bromodomain protein Brd4 insulates chromatin from DNA damage signalling. Nature. 2013;498(7453):246–50. [PubMed: 23728299]
46. Helleday T, Petermann E, Lundin C, Hodgson B, Sharma RA. DNA repair pathways as targets for cancer therapy. Nature reviews Cancer. 2008;8(3):193–204. [PubMed: 18256616]
47. Puigvert JC, Sanjiv K, Helleday T. Targeting DNA repair, DNA metabolism and replication stress as anti-cancer strategies. The FEBS journal. 2016;283(2):232–45. [PubMed: 26507796]
48. Farmer H, McCabe N, Lord CJ, Tutt AN, Johnson DA, Richardson TB, et al. Targeting the DNA repair defect in BRCA mutant cells as a therapeutic strategy. Nature. 2005;434(7035):917–21. [PubMed: 15829967]
49. Fong PC, Boss DS, Yap TA, Tutt A, Wu P, Mergui-Roelvink M, et al. Inhibition of poly(ADP-ribose) polymerase in tumors from BRCA mutation carriers. The New England journal of medicine. 2009;361(2):123–34. [PubMed: 19553641]
50. Toledo LI, Murga M, Zur R, Soria R, Rodriguez A, Martinez S, et al. A cell-based screen identifies ATR inhibitors with synthetic lethal properties for cancer-associated mutations. Nature structural & molecular biology. 2011;18(6):721–7.
51. Goundiam O, Gestraud P, Popova T, De la Motte Rouge T, Fourchotte V, Gentien D, et al. Histo-genomic stratification reveals the frequent amplification/overexpression of CCNE1 and BRD4 genes in non-BRCAness high grade ovarian carcinoma. International journal of cancer. 2015;137(8):1890–900. [PubMed: 25892415]
52. Crafter C, Vincent JP, Tang E, Dudley P, James NH, Klinowska T, et al. Combining AZD8931, a novel EGFR/HER2/HER3 signalling inhibitor, with AZD5363 limits AKT inhibitor induced feedback and enhances antitumour efficacy in HER2-amplified breast cancer models. International journal of oncology. 2015;47(2):446–54. [PubMed: 26095475]
53. Lehar J, Krueger AS, Avery W, Heilbut AM, Johansen LM, Price ER, et al. Synergistic drug combinations tend to improve therapeutically relevant selectivity. Nature biotechnology. 2009;27(7):659–66.

54. Kilkenny C, Browne WJ, Cuthill IC, Emerson M, Altman DG. Improving bioscience research reporting: The ARRIVE guidelines for reporting animal research. Journal of pharmacology & pharmacotherapeutics. 2010;1(2):94–9. [PubMed: 21350617]

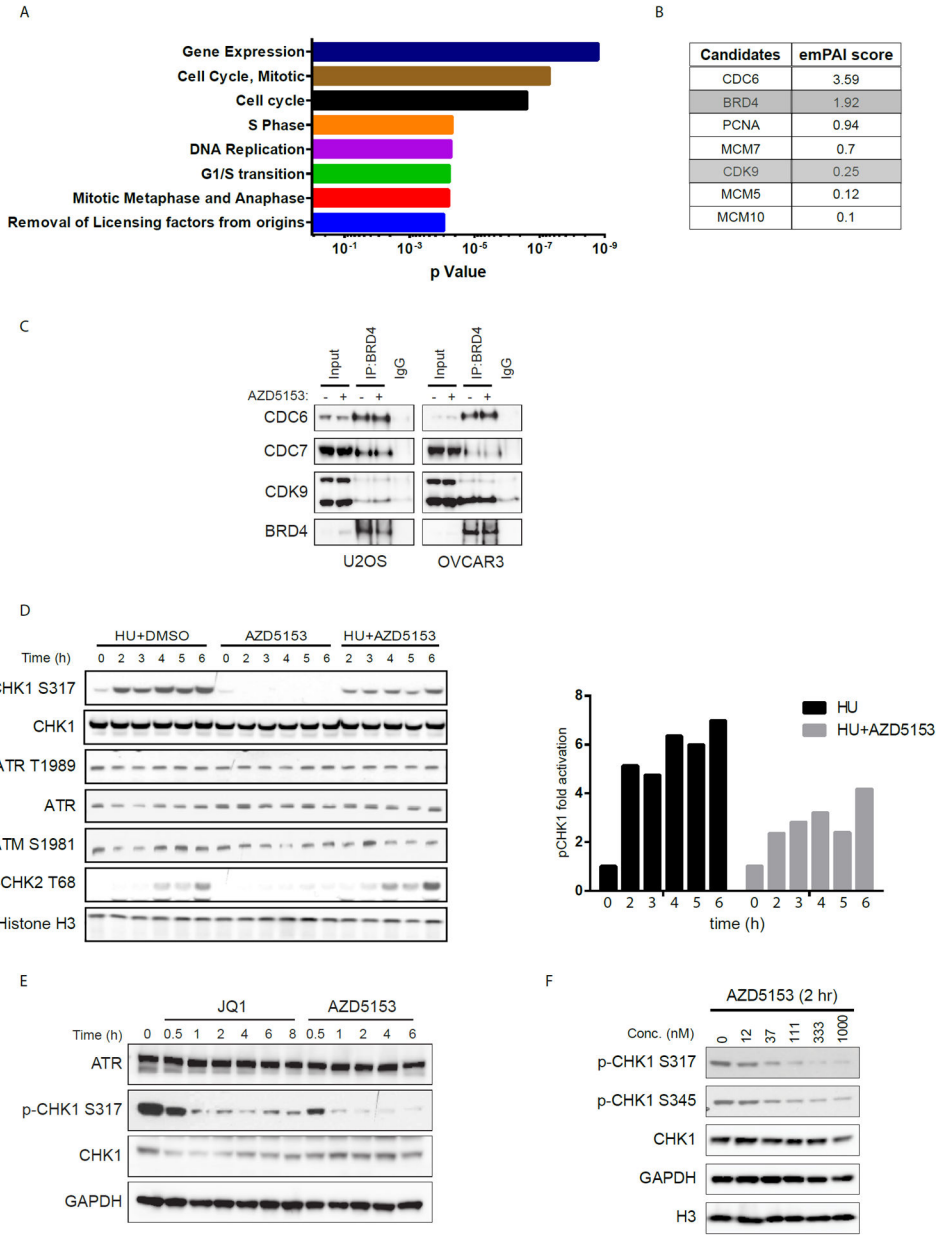

Candidates	emPAI score
CDC6	3.59
BRD4	1.92
PCNA	0.94
MCM7	0.7
CDK9	0.25
MCM5	0.12
MCM10	0.1

Figure 1. BRD4 interacts with the pre-replication complex and regulates DNA replication checkpoint response.

A. Pathway enrichment analysis of BRD4 interacting proteins identified in immunoprecipitation and mass spectrometry analysis from U2OS cells (Database: ConsensusPathDB).

B. Identified pre-replication complex components that interacted with BRD4 and their corresponding emPAI scores. Only proteins with emPAI score >0.1 are listed. Also listed are CDK9, a component of the pTEFb complex and a known BRD4-interacting protein, and the bait protein BRD4.

C. Immunoprecipitations of BRD4 or IgG control were performed in U2OS and OVCAR3 cells treated with or without AZD5153 (500 nM, 2h treatment). Western blot analysis of the

resulting immuno-complexes confirms association between BRD4 and the pre-replication complex.

D. Western Blot analysis showing time-dependent responses of phospho- and total CHK1, phospho- and total ATR, phospho-ATM, and phospho-CHK2 under replication stress conditions induced by hydroxyurea (HU, 10 mM) with or without the presence of AZD5153 (500 nM) in U2OS cells. Bar plots on the right depict the relative pCHK1 intensity induced by HU over time and the dampened pCHK1 activity with AZD5153 treatment.

E. Western Blot analysis of ATR and CHK1 signaling activities in OVCAR3 cells following treatment with JQ1 (2 μM) or AZD5153 (500 nM) for indicated periods of time.

F: Western Blot analysis of OVCAR3 cells treated with increasing concentrations of AZD5153 (2 hour treatment).

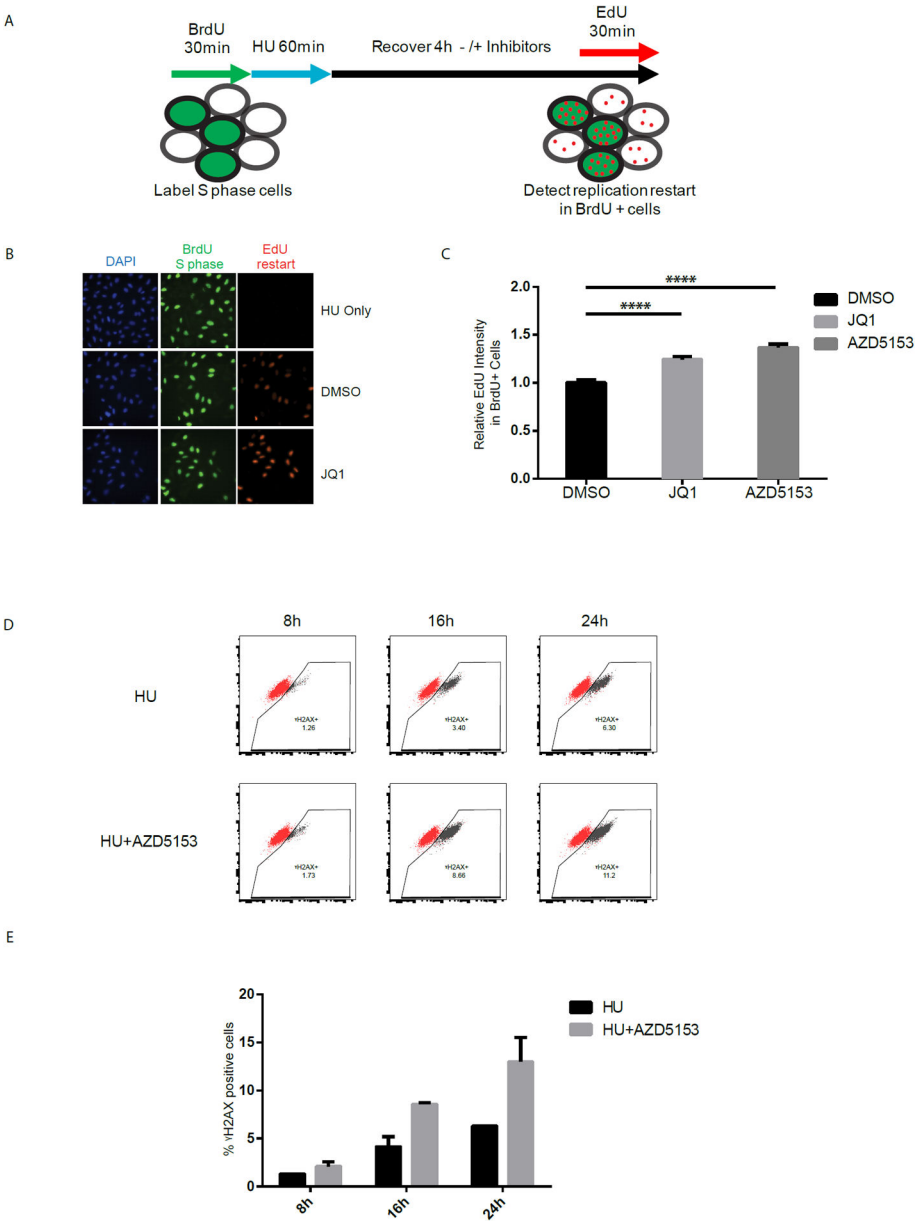

Figure 2. Inhibition of BRD4 leads to aberrant DNA replication re-initiation and sensitization to replication stress-inducing agents.

A. Schematic of DNA replication re-initiation/restart assay. U2OS cells are first pulse-labeled with BrdU to identify cells in replication phase (S phase), and then treated with HU to induce replication stress. After one hour of HU treatment, HU is removed and cells are replenished with fresh medium with or without BETi (JQ1 or AZD5153). New DNA replication is detected with EdU pulse labeling after a 4-hour recovery.

B. Representative images of U2OS in replication re-initiating/restart assays. All cell nuclei are identified with DAPI staining. BrdU labels cells that are in S phase, whereas EdU staining indicates recovered DNA replication activity after HU treatment in these cells. In cells labeled as HU only, HU was not washed-out. Representative images of HU-, DMSO- and JQ1-treated samples are shown.

C. Average EdU intensity (per cell) in BrdU positive cells indicates DNA replication re-initiation under various experimental conditions (same as B, JQ1 2 μM, AZD5153 500 nM). All results are normalized to DMSO-treated control group (**** $p<0.0001$).

D. Pseudocolor plots of U2OS treated with HU or HU+AZD5153 analyzed by flow cytometry. γH2AX positive gate (outlined area) is determined based on unstained controls. γH2AX positive cells under each treatment condition are highlighted in gray. (HU 2 mM, AZD5153 500 nM, representative images are shown)

E. Quantification for percentage of γH2AX positive population in U2OS cells treated with HU without or with AZD5153 for increasing amounts of time (same as D, N=3).

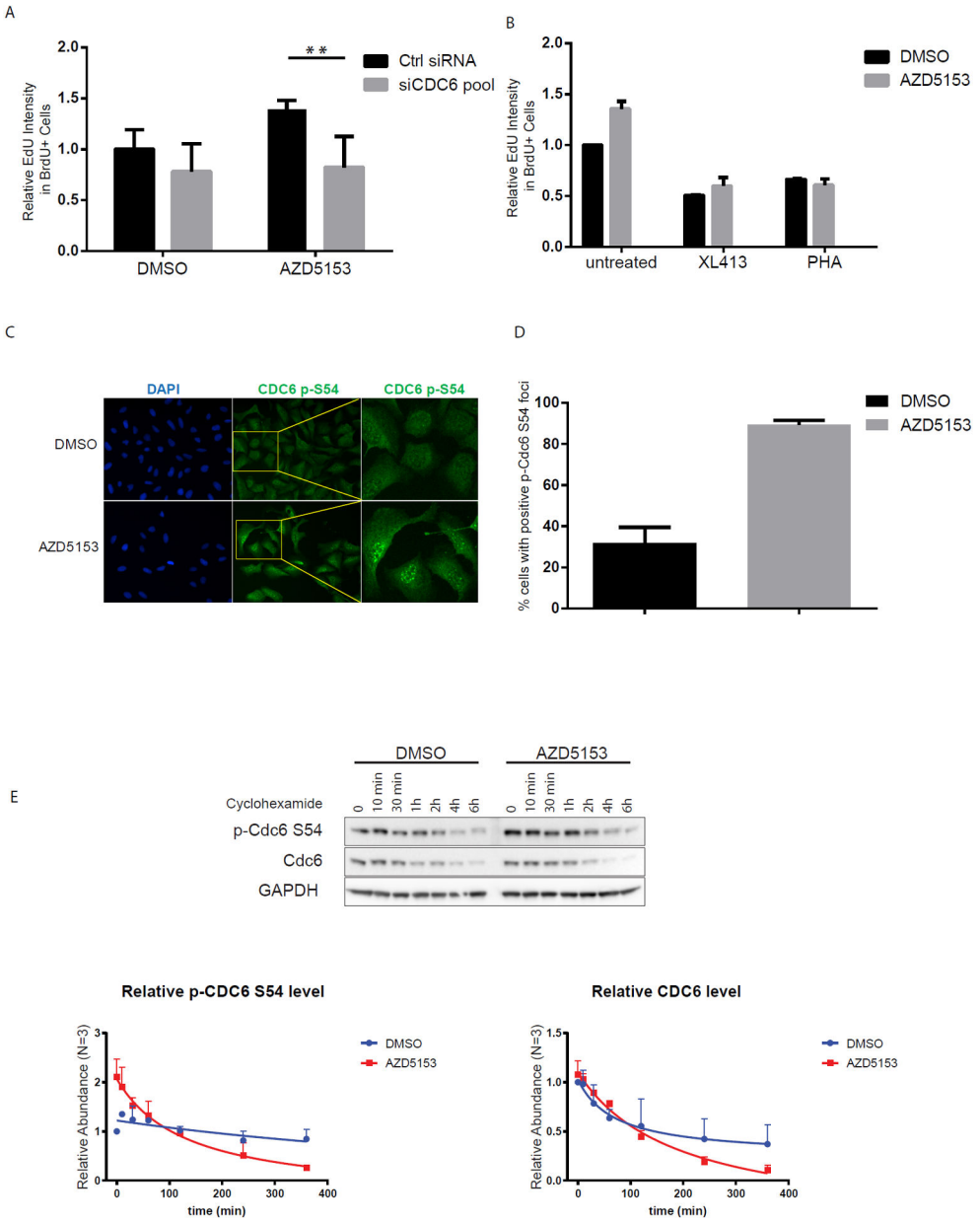

Figure 3. BETi leads to defective replication stress response through deregulated CDC6 activity.

A. Quantification of relative EdU incorporation in U2OS cells transfected with control siRNA or a pool of four different CDC6 siRNA as measured in the DNA replication re-initiation/restart assay with or without AZD5153 treatment. (** p=0.0055)

B. Effects of two CDC7 inhibitors, XL413 (5 μM) and PHA767491 (5 μM), on DNA replication re-initiation/restart after HU treatment in the presence or absence of AZD5153.

C. Representative images of U2OS cells stained for phospho-CDC6 (S54) with or without 2-hour AZD5153 treatment (500 nM). Selective regions are zoomed in to show phospho-CDC6 foci.

D. Quantification of C for percentage of U2OS cells stained positive for phospho-CDC6 (S54) foci following a 2-hour AZD5153 treatment.

E. U2OS cells were treated with DMSO or AZD5153 (500nM) followed by cycloheximide chase to examine protein turnover rate. Expression levels of phospho-CDC6 Ser54 and total CDC6 at different time points following cycloheximide chase were examined by western blot. Quantification of phospho-CDC6 Ser54 and total CDC6 levels was graphed at the bottom (N=3).

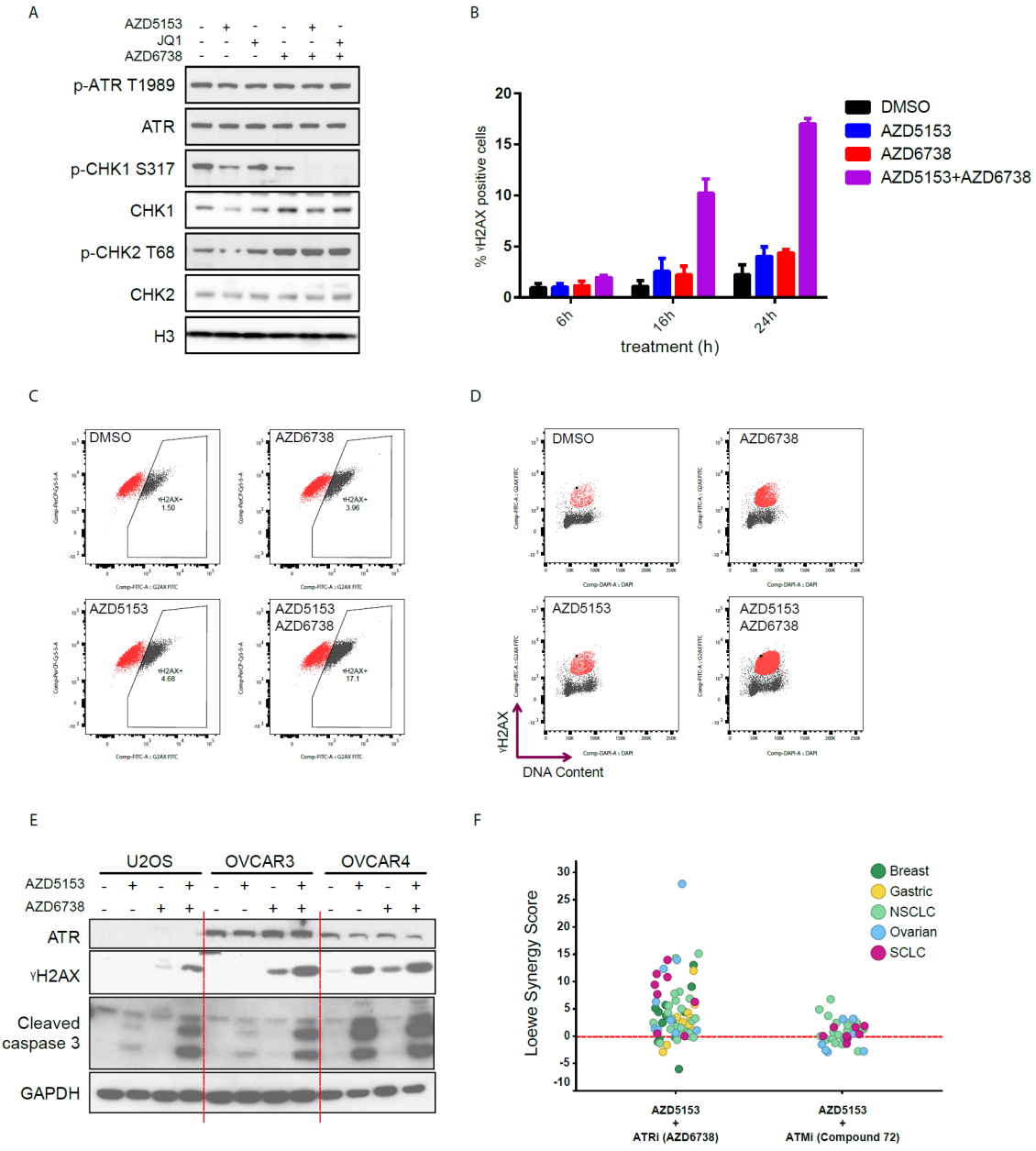

Figure 4. BETi and ATRi induce DNA damage and apoptosis in a synergistic manner.

A. Western Blot analysis of U2OS cells treated with BETi (JQ1 or AZD5153), ATRi (AZD6738), or combination of BETi and ATRi. Greater inhibition of phospho-CHK1 is seen with combination treatment compared to either single agent treatment alone. (AZD5153 250 nM, JQ1 2 μM, AZD6738 100 nM, 24h treatment)

B. OVCAR3 cells were treated with BETi (AZD5153, 500nM), ATRi (AZD6738, 500 nM) or combination of AZD5153 and AZD6738 for indicated periods of time before being fixed and stained for γH2AX for flow cytometry analysis. Percentage of cells showing positive γH2AX staining at different time points are graphed (N=3).

C. Pseudocolor plots showing γH2AX positive population after 24 hours of indicated treatment conditions (Same as B). γH2AX positive gate (outlined area) is determined based on unstained controls. γH2AX positive population are highlighted in grey.
D. Pseudocolor plots showing DNA content (x-axis) and γH2AX intensity (y-axis) distribution of OVCAR3 cells following a 24-hour treatment of indicated agents (Same as C). Note accumulation of γH2AX positive population between 2N and 4N DNA content (highlighted in red), indicating accumulated DNA damage in S phase cells.
E. Western Blot analysis of U2OS, OVCAR3 and OVCAR4 cells after treatment with AZD5153, AZD6738, or AZD5153+AZD6738 combo (AZD5153 500 nM, AZD6738 500 nM, 24h treatment). γH2AX and cleaved-caspase 3 are used as makers for DNA damage and apoptosis, respectively.
F. Combination testing was performed in a panel of breast, small cell lung, non-small cell lung, ovarian, and gastric cancer cell lines. Cell viability was measured after combination treatment of AZD5153 with ATR inhibitor AZD6738 (67 cell lines), or with ATM inhibitor (Compound 72) (40 cell lines). Combination synergy scores were calculated using Loewe's Model and the results are graphed as scatter plots showing the distribution of cell lines according to their synergy scores. Positive synergy score indicates greater than additive effects of two compounds in cell killing. Dashed line marks the synergy score of zero.

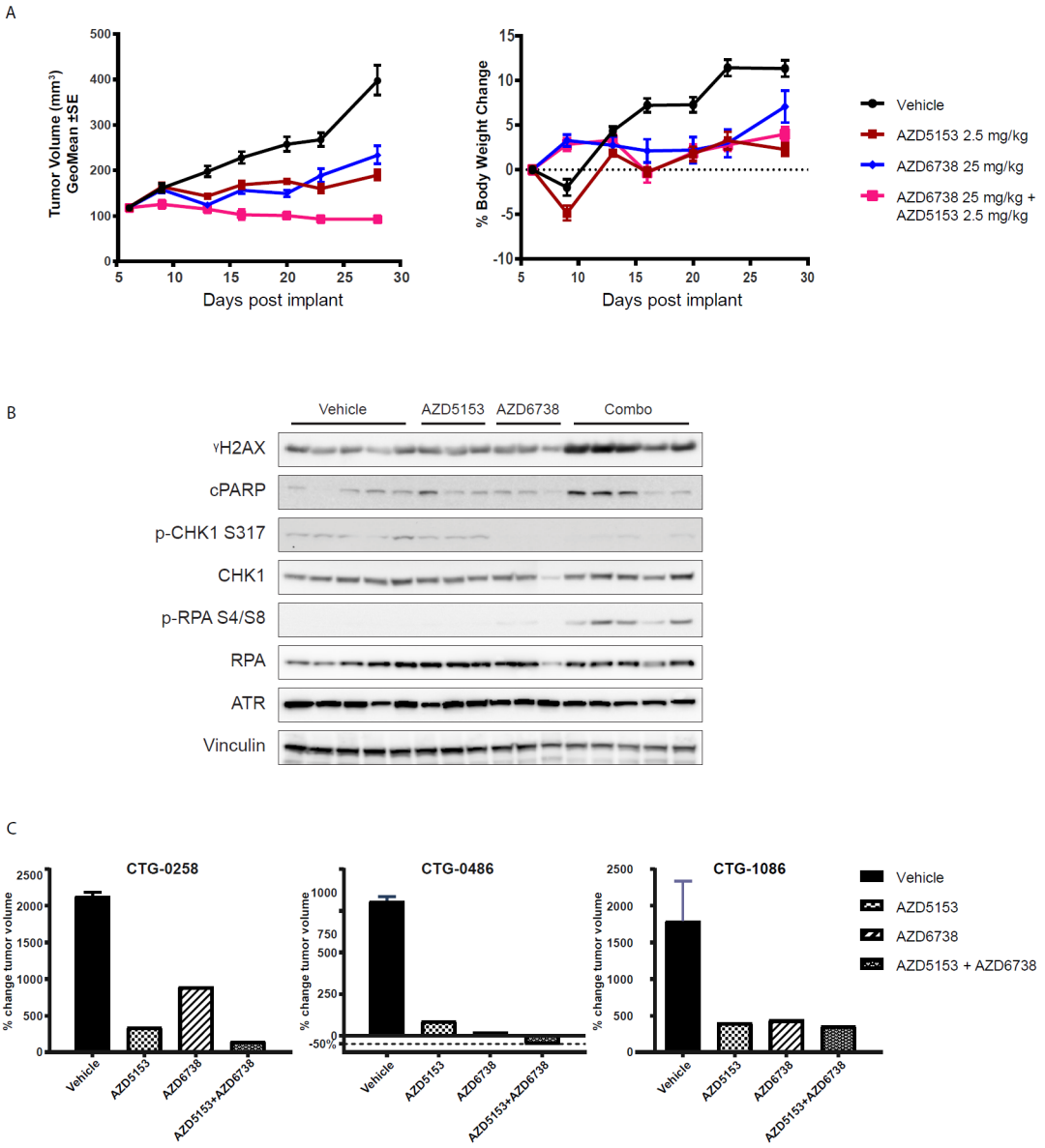

Figure 5. Concurrent BET and ATR inhibition inhibits ovarian tumor growth *in vivo*.

A. OVCAR3 cells were injected subcutaneously into C.B.−17 *scid* mice and allowed to grow for 6 days. Tumor-bearing mice randomized into the following treatment groups (n = 10/group) were orally administered vehicle once daily, 2.5 mg/kg AZD5153 once daily, 25 mg/kg AZD6738 once daily, or a combination of AZD5153 and AZD6738 once daily for 21 days. Data values for tumor volumes are represented as geometric mean ± SEM. Data values for % body weight change are represented as mean ± SEM of each treatment group.

B. Western blot analysis of indicated markers in OVCAR3 xenograft tumor samples after four repeated doses.

C. Bar graphs representing tumor volume change in N=1 testing of ovarian PDX models. For each model, tumor-bearing mice were randomized into each treatment group and were orally administered vehicle once daily (n = 3), 2.5 mg/kg AZD5153 once daily (n = 1), 25 mg/kg AZD6738 once daily (n = 1), or a combination of AZD5153 and AZD6738 once

daily (n = 1) for 28 days. At the end of the treatment period, tumor volume was measured and % change in tumor volume was calculated.